

AD-A102 153

THE FREE ELECTRON LASER SIDEBAND INSTABILITY  
RECONSIDERED(U) NAVAL RESEARCH LAB WASHINGTON DC  
S RIVOPOULOS ET AL. 1986

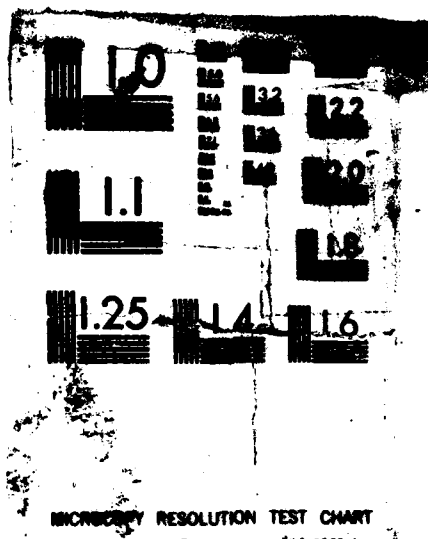
1/1

UNCLASSIFIED

F/G 9/3

NL





DTIC FILE COPY

AD-A182 153

THE FREE ELECTRON LASER SIDEBAND INSTABILITY RECONSIDERED

S. Riyopoulos\* and C. M. Tang

Naval Research Laboratory

Washington, DC 20375-5000

1986

Abstract

delta sub gamma

→ The one-dimensional fast-time averaged Hamiltonian is derived in a free electron laser (FEL) for electrons passing through a constant wiggler and a radiation field. The exact unperturbed orbits without sidebands are obtained for all particles and arbitrary separatrix width  $\delta\gamma$ . Integration in action-angle variables of the linearized Vlasov equation with perturbing sidebands over the unperturbed orbits yields the sideband gain for both trapped and untrapped particles. The unperturbed distribution  $f_0$  is in an adiabatic equilibrium with the main signal field. It is found that upper and lower sidebands that are symmetric relative to the FEL frequency have opposite growth rates. There is no differentiation in the magnitude of the gain between upper and lower sidebands. The stability is determined by the sign of  $df_0/d\omega_b$ , i.e., the relative population of oscillation quanta  $h_b$ ,  $\omega_b$  = bounce frequency around resonance. The shear  $d\omega_b/dJ$ , where  $J$  is the action variable, is stabilizing and distributions with gradients  $df_0/dJ$  localized near the separatrix have the minimum growth rates. The structure and scaling of the unstable spectrum are different from previous results obtained for electrons localized at the bottom of the ponderomotive well.

sub c

omega sub b

\* Science Applications Intl. Corp., McLean VA.

DTIC  
ELECTE  
JUN 29 1987  
S A D

## I. INTRODUCTION AND SUMMARY

The growth of parasitic modes at frequencies near the main signal frequency during high power FEL operation was theoretically predicted<sup>1,2</sup> in early 1980's. Since then there has been ample numerical<sup>3,4</sup> and experimental<sup>5,6</sup> evidence of sideband excitation in constant wiggler FELs. Unstable modes in variable wiggler FELs have also been observed in simulations<sup>7-9</sup> and recently in experiment<sup>10</sup>. Sidebands degrade the main signal efficiency and optical quality by channeling a considerable fraction of the power into parasitic frequencies. The performance of the mirrors in an oscillator can be harmed from the modulation of the wave envelope caused by the sidebands. Last, but not least, interaction among nearby sidebands above a certain amplitude may lead to chaotic particle motion, loss of trapping and incoherent radiation.

The above have stimulated a considerable amount of theoretical work focused on sideband growth. Simple one-dimensional configurations that are analytically tractable have been used to model the situation. Two lines of approach have been considered. The single particle picture regards the particle trajectories as functions of the initial conditions and computes the gain by ensemble averaging over initial distributions<sup>7-9</sup>. The alternative approach assumes some adiabatic equilibrium between the particles and the main signal and examines the stability of the perturbations induced by the sidebands, solving the

kinetic equation<sup>11,12</sup>. Because of the equilibrium assumption the kinetic method is more appropriate for FEL operation as an amplifier.

In both treatments so far, analytic results have been obtained only for particles localized near the bottom of the ponderomotive well. This implies the following limitations: The sideband spectrum becomes discrete

$$\omega_s = \omega_r \pm (k_r/k_w) n \omega_b(0), \quad k_r/k_w \approx 2\gamma_z^2, \quad (1)$$

where  $\omega_b(0)$  is the bounce frequency at the bottom of the ponderomotive well,  $k_r$   $k_w$  are the radiation and wiggler wave numbers respectively and  $\gamma_z = (1 - v_z^2/c^2)^{-1/2}$ . The contribution from untrapped particles and trapped particles away from the bottom is neglected. The effect of the shear  $d\omega_b/dJ$ , where the action  $J$  parametrizes the distance from the centre of the separatrix  $J=0$ , is lost. Finally no predictions can be made about the saturation level of potentially unstable modes.

Here canonical formalism is introduced by expressing the unperturbed particle orbits in terms of action-angle variables. The unperturbed orbits are of course the fast time averaged "synchrotron" oscillations of the electrons in the potential well formed by the combined action of the wiggler and the radiation signal. The perturbed kinetic equation is solved in action space, starting from an equilibrium extending over all trapped and untrapped electrons. It is found that:

(a) the spectrum becomes continuous replacing  $\omega_b(0)$  by  $\omega_b(J)$  in Eq. (1). The modes located at the peaks of the unstable spectrum grow faster, emerging as the discrete spectrum that is observed in simulations.



Py	
Distribution/	
Availability Codes	
Dist	Avail and/or Special
A-11	

(b) More than one group of particles are in resonance with a given sideband frequency  $\omega_s$  through different harmonics of their bounce frequency and contribute to the growth rate.

(c) The shear  $da_0/dJ$  is stabilizing. Distributions with gradients  $df_0/dJ$  localized near the separatrix are found to have the minimum growth rates because of the high shear there. This type of distribution is relevant to FEL's with tapered wigglers.

(d) The gain is proportional to  $[df(J)/da_0(J)]$ , the relative population in oscillation quanta around resonance, in agreement with the quantum mechanical interpretation.

(e) Upper and lower sidebands located symmetrically around the main signal frequency have opposite gains (complementary stability). Therefore one mode is always unstable. There is no stable distribution  $f_0(J)$  except the trivial one  $df_0/dJ=0$ .

(f) For any smooth distribution, of finite  $df_0/dJ$ , electrons at the bottom of the well have a negligible effect on stability.

(g) Previous results, finding lower sidebands having an inherently larger gain than upper sidebands, are relevant only to the limiting case of a singular  $\delta$ -function distribution  $f_0(J)=\delta(J)$ . This case is unrealistic because a wide, smooth initial distribution in action  $f_0(J)$  corresponds to even an ideal cold beam distribution in momentum  $f_0(p)=\delta(p-p_0)$ .

The nonlinear saturation levels for the unstable modes and the amplitude for stochastic transition can also be derived from our formalism and will be addressed in future work.

## II. COMPUTATION OF THE GAIN

We consider a linearly polarized wiggler of constant wavelength  $2\pi/k_v$  and constant amplitude  $A_v$  and plain monochromatic waves for the main signal and the sideband. The total vector potential is given by  $A=A_y(z,t)e_y$  with

$$A_y(z,t) = A_v \cos k_v z + A_r \cos(k_r z - \omega_r t) + A_s \cos(k_s z - \omega_s t) \quad (2)$$

where the subscripts v, r and s stand for wiggler, main radiation and sideband respectively,  $A_r$ ,  $A_s$ , are constant and  $A_r \gg A_s$ . Our Hamiltonian is one-dimensional non autonomous because the canonical momenta

$$P_x = p_x, \quad P_y = p_y - \frac{e}{c} A_y(z,t) \quad (3)$$

are constants of motion that can be conveniently set to zero. We switch to the time averaged coordinates  $P_z = \langle P_z \rangle$  and  $z = \langle z \rangle$  through the appropriate canonical transformation, choosing a generating function that kills the fast oscillating terms due to the wiggling motion (see Ref. 13). Introducing the new variables

$$P = \hat{P}_z / (k_r + k_v), \quad \psi = (k_r + k_v) \hat{z} - \omega_r t$$

and keeping only linear terms in the small amplitude  $a_s$ , the averaged interaction Hamiltonian becomes

$$H(P, \psi; t) = \{H^2 + (k_r + k_v)^2 P^2 - a_v a_r \cos \psi - a_v a_s \cos(\psi - \delta_s t)\}^{1/2} \quad (4)$$

Here time is normalized to  $\omega_r^{-1}$ , length to  $k_r^{-1}$ , velocity to  $c$ , mass to  $m_e$ ,  $a_1 = eA_1/m_e c^2$  and  $H^2 = 1 + (a_v^2 + a_r^2)/2$ . Although  $k_r = \omega_r = 1$  in the above units we will write them explicitly to avoid confusion. The term  $\delta_s$  in Eq. (4) signifies the Doppler shifted frequency departure of the sideband from the main signal

$$\delta_s = (k_v/k_r) (\omega_s - \omega_r). \quad (5)$$

The terms proportional to  $a_v a_r$  and  $a_v a_s$  are the ponderomotive potentials caused by the beating together of the wiggling motion with the signal and the sideband field respectively.

When  $a_s = 0$  the Hamiltonian  $H_0(P, \psi)$  is exactly integrable. The unperturbed trajectories, shown in Fig. 1(a), are given by

$$H_0(P, \psi) = K$$

with the constant  $K$  determined from the initial conditions  $K = H_0(P_0, \psi_0)$ . These trajectories take the simplest possible form expressed in terms of the action angle variables  $(J, \theta)$

$$\begin{aligned} J(t) &= J_0 = \text{const.}, \\ \theta(t) &= \theta_0 + \omega_0(J)t, \\ \omega_0(J) &= dH_0(J)/dJ, \end{aligned} \quad (6)$$

where  $J$  is the area in phase space enclosed by an orbit divided by  $2\pi$ . In the above variables the width of the separatrix  $w$  is given by



$v=J_{sep}$  with  $J_{sep}$  the value of action at the separatrix. The relation between new  $(J, \theta)$  and old  $(P, \phi)$  variables is expressed by

$$\begin{aligned}
 J &= \begin{cases} \frac{2}{\pi} \left( \frac{G}{2} \right)^{1/2} \frac{1}{A} [E_2(\lambda) - (1-\lambda^2)E_1(\lambda)], & \lambda^2 < 1 \\ \frac{4}{\pi} \left( \frac{G}{2} \right)^{1/2} \frac{\lambda}{A} E_2(1/\lambda), & \lambda^2 > 1 \end{cases} \\
 \sin \frac{\phi}{2} &= \begin{cases} \lambda \operatorname{sn} \left[ \frac{2}{\pi} E_1(\lambda) \theta \right], & \lambda^2 < 1 \\ \operatorname{sn} \left[ \frac{1}{\pi} E_1(1/\lambda) \theta \right], & \lambda^2 > 1 \end{cases}
 \end{aligned} \tag{7}$$

with  $E_1, E_2$  the complete elliptic integrals of the first and second kind and  $\operatorname{sn}$  the Jacobi elliptic sine function. The trapping parameter  $\lambda^2$  is given by

$$\begin{aligned}
 \lambda^2 &= (F+G)/2G, \\
 F &= (k_r + k_v)^2 (K^2 - H^2), \\
 G &= a_v a_r [(k_r + k_v)^2 - 1],
 \end{aligned} \tag{8}$$

and we have  $\lambda^2 < 1$ ,  $\lambda^2 > 1$  for trapped and untrapped particles respectively. The three constants of the motion  $\lambda^2$ ,  $K$  and  $J$  are mutually dependent and any one of them defines uniquely a trajectory. The bounce frequency is found from Eqs. (6), (7) and (8)

$$a_b(J) = \begin{cases} a_b(0) \frac{\pi}{2E_1(\lambda)}, & \lambda^2 < 1 \\ a_b(0) \frac{\pi\lambda}{E_1(1/\lambda)}, & \lambda^2 > 1 \end{cases} \quad (9)$$

with

$$a_b(0) = (G/2)^{1/2} \frac{(k_v + k_r)^2 - 1}{(k_r + k_v)^2 K} = \frac{1}{\gamma_z} (a_v a_r k_v k_r)^{1/2}.$$

We now perform a linear expansion of the Hamiltonian Eq. (4) in the small sideband amplitude  $a_s$  followed by a decomposition of the perturbing term  $\cos[\psi(\theta) - \delta_s t]$  into harmonics of the synchrotron oscillation to obtain

$$H(J, \theta) = H_0(J) + \sum_{n=0}^{\infty} \{ h_n^+(J) \cos(n\theta + \delta_s t) + h_n^-(J) \cos(n\theta - \delta_s t) \},$$

$$h_n^{\pm}(J) = \frac{a_v a_r}{H_0(J) + P_r} Q_n^{\pm}(J). \quad (10)$$

The coefficients  $Q_n(J)$  are obtained by contour integration in the complex plane using the double periodicity properties of the Jacobi elliptic functions,

$$Q_n^{\pm} = -(\pm 1)^n \frac{n\pi^2}{E_1^2(\lambda)} \frac{q^{\frac{n}{2}}}{1 - (-q)^n}, \quad q = \exp\left(\frac{\pi E_1'(\lambda)}{E_1(\lambda)}\right), \quad \lambda^2 < 1$$

$$Q_n^{\pm} = -\frac{n\pi^2 \lambda^2}{E_1^2(1/\lambda)} q^n \left( \frac{1}{1 - q^{2n}} \pm \frac{1}{1 + q^{2n}} \right), \quad q = \exp\left(\frac{\pi E_1'(1/\lambda)}{E_1(1/\lambda)}\right), \quad \lambda^2 < 1$$

$Q_n(J)$  tends to 0 as  $J$  tends to either 0 or  $\infty$  while the maximum occurs at the separatrix  $\lambda^2 = 1$ .  $Q_n(J)$  becomes progressively smaller with

increasing  $n$  everywhere except in the vicinity of the separatrices. That limits the number of harmonics to be considered for instabilities localized away from the separatrix. The perturbed equations of motion in the standard form read

$$\begin{aligned}\frac{d}{dt} J &= \sum_{n=0}^{\infty} n \{ h_n^+(J) \sin(n\theta + \delta_s t) + h_n^-(J) \sin(n\theta - \delta_s t) \}, \\ \frac{d}{dt} \theta &= \omega_b(J) + \sum_{n=0}^{\infty} \left\{ \frac{dh_n^+}{dJ} \cos(n\theta + \delta_s t) + \frac{dh_n^-}{dJ} \cos(n\theta - \delta_s t) \right\}.\end{aligned}\quad (11)$$

The gain  $g_s$  for a given sideband is determined by the energy balance equation

$$\frac{d}{dt} a_s^2 = 2g_s a_s^2 = \frac{1}{2} \left\{ \frac{4\pi ic}{\omega_s} \langle j_y a_s^* \rangle + cc \right\}. \quad (12)$$

The bracket  $\langle \rangle$  denotes the average of a quantity  $\langle f \rangle = 1/T \int_0^T f(t) dt$  over the fast time scale  $T = 2\pi/k_v v_e \ll T_b = 2\pi/\omega_b$ , and  $j_y$  is the transverse current

$$j_y(z, t) = en_b \iint v_y \delta f(J, \theta; t) dJ d\theta, \quad (13)$$

with

$$v_y = \gamma^{-1} p_y = -(e/\gamma mc) A_y(z, t).$$

For small sideband signal  $\delta f$  is the perturbed distribution  $f_1$  under the Hamiltonian flow Eqs. (11)

$$\frac{\partial f_1}{\partial t} + \omega_b(J) \frac{\partial f_1}{\partial \theta} = - \frac{dJ}{dt} \frac{df_0}{dJ}, \quad (14)$$

where  $f_0$  is the equilibrium distribution along the unperturbed orbits  $df_0/dt=0$ . Any distribution  $f_0(J)$  depending on  $J$  alone is invariant under Eqs. (6)

$$\frac{d}{dt} f_0 = \frac{dJ}{dt} \frac{df_0}{dJ} = 0$$

thus  $f_0$  is not uniquely defined.

Solving Eq. (14) for  $f_1$ , then substituting Eqs. (10) and (13) into (12) and time-averaging one obtains the final result

$$g^{\pm} = \mp a_v^2 \frac{\omega_r}{\omega_s} \frac{\pi^2 \omega_{pb}^2}{8 \gamma_r \omega_r^2} \sum_n \frac{|Q_n^{\pm}(J)|^2}{|H_0(J_n) + \gamma_r|} \left( \frac{df_0}{dJ} \right)_{J_n} \left( \frac{d\omega_b}{dJ} \right)_{J_n}^{-1}, \quad (16)$$

with  $\omega_{pb}$  the beam plasma frequency. The superscript + or - corresponds to upper  $\omega_s > \omega_r$  and lower  $\omega_s < \omega_r$  sideband respectively.  $J_n$  is given implicitly by the resonant condition

$$\pm n \omega_b(J_n) = (k_v/k_r) (\omega_s - \omega_r), \quad (17)$$

as illustrated in Fig. 1(b). The sum over  $n$  on the right-hand side of Eq. (16) includes the contribution from all resonant groups of particles. The action  $J_n$  in Eq. (17) labels the orbit having the  $n$ -th harmonic of the local bounce frequency in resonance with the sideband. The gain is determined by the slope of the distribution function  $f_0$  near these resonant orbits  $J \approx J_n$ .

### III. RESULTS AND CONCLUSIONS

The opposite signs in the right-hand side of Eq. (16) denote that upper and lower sidebands located symmetrically around the main signal  $|\omega_s^+ - \omega_r| = |\omega_s^- - \omega_r|$  have opposite growth rates,  $g^+/g^- = -1 + O(\delta\omega/\omega_r)^2$ . The physical reason is connected with quantum mechanical considerations. The practical implication is that one sideband is always unstable except in case of trivial equilibrium  $df_0/dJ=0$ . It also reveals that, once destabilized, upper and lower modes have growth rates of equal magnitude and are equally dangerous. We clarify that, in general, the opposite signs do not imply that all upper sidebands have the same kind of stability, opposite to the stability of all lower sidebands. Depending upon  $f_0$  stability may change sign between two upper (or lower) frequencies because the slopes  $df_0/dJ_n$  change as the location of the resonant  $J_n$ 's shift with  $\omega_s$ .

For a monotonic distribution  $f_0$  we observe that trapped and untrapped particles yield opposite contributions to a given mode because  $d\omega_b/dJ$  changes sign across the separatrix. If trapped particles are stabilizing untrapped are destabilizing and vice versa. High shear is stabilizing tending to reduce the magnitude of the gain  $g_s$ . This is expected as the number of resonant orbits is inversely proportional to  $|d\omega_b/dJ|$ . Shear tends to infinity near the separatrix thus the modes generated by electrons orbiting near the separatrix, corresponding to small  $|\omega_s - \omega_r| \ll (k_r/k_v)n\omega_b(0)$ , have the smallest growth rates. Modes coming from electrons near the center  $J_n \approx 0$  with

$|\omega_s - \omega_r| = (k_r/k_v) n \omega_b(0)$  have also small growth rates as the coefficients  $Q_n(J)$  tend to zero there. In particular, given any smooth distribution  $f_0(J)$ , electrons exactly at the bottom of the well have a null contribution to the instability. It takes a singular distribution of infinite gradient at  $J=0$  to create an instability from electrons exactly at the center of the separatrix. The shear is generally higher for untrapped particles thus the trapped ones usually dominate the instability.

Although Eq. (16) was obtained on purely classical arguments it nevertheless admits the correct quantum mechanical interpretation. Expressing  $(df_0/dJ)(d\omega_b/dJ)^{-1}$  as  $df_0/d\omega_b$  we observe that the gain  $g_s$  is proportional to the difference in population of oscillation quanta  $\hbar\omega_b$  between the energy levels across the resonance. A more detailed explanation for the opposite signs in Eq. (16) is given in Ref. 13.

The normalized gain  $g_s/\omega_r$  is plotted against the percentage mismatch  $(\omega_s - \omega_r)/\omega_r$  for both upper and lower sidebands in Figs. 2 and 4. The contribution up to the third harmonic  $n \leq 4$  in Eq. (16) is included in these plots. The parameters chosen correspond to a wiggler wavelength  $\lambda_v = 3$  cm,  $a_v = 5$ , main signal strength  $a_s = 5 \times 10^{-4}$  beam energy of 11.43 MeV ( $\beta = 0.999$ ,  $\gamma = 22.37$ ) and current density  $j = 100$  A/cm<sup>2</sup> (beam density  $6.25 \times 10^{10}$  cm<sup>-3</sup>). The equilibrium distribution is a Gaussian  $f_0(J) = (1/2\pi D^2)^{1/2} \exp(-(J - J_0)^2/2D^2)$  centered halfway inside the island,  $J_0 = w/2$ , and of width  $D$  equal to half the separatrix distance  $D = w/2$ , with  $w = J_{sep}$ . We plot the contribution of only the fundamental,  $n=1$  in Eq. (16), in Fig. 2(a) adding the first harmonic  $n=2$  in (b) the second harmonic in (c) and the third harmonic in (d). New unstable bands emerge with each harmonic, while the gain for already unstable bands

is modified. For example we observe two upper and two lower unstable bands in (b) but only one upper and three lower bands in (d). We find the contributions from higher than the third harmonics  $n > 4$  generally negligible. The upper frequency  $\omega_s > \omega_r$  and the lower frequency  $\omega_s < \omega_r$  parts of the unstable spectrum come from the regimes of negative and positive slope  $df_0/d\omega_b$  respectively, shown in Fig. 3. The lower sideband growth is peaking at frequencies corresponding to  $n\omega_b(J_{\max})$  with  $J_{\max}$  the value maximizing  $df_0/d\omega_b(J)$ . The peaks for the upper sideband growth, however, do not occur at  $J=0$  that minimizes  $df_0/d\omega_b(J)$ , but at  $J$  halfway inside the negative slope regime. This is because  $Q_n(J)$  and consequently  $g_s$  are zero at  $J=0$ , showing the negligible contribution from electrons at the bottom of the well. The analogous effect in plasma physics is the elimination of the thermal effects when  $\rho_L$  goes to zero. In any case the most unstable modes are far from the frequencies  $|\omega_s - \omega_r| = (k_r/k_w)n\omega_b(0)$  pointed by the arrows in Fig. 2(d).

Since sidebands can not be shut out completely it remains debatable whether a distribution function can be tailored experimentally to minimize their growth rate. From the previous discussion a flat distribution inside the trapped regime with sharp gradients localized at the separatrix seems the appropriate choice. Instabilities will then localize near the separatrix and the gain will be suppressed by the strong shear. To check this we plot the growth rates from Eq. (16) for two types of distributions  $f_0(J)$ : (i) Two Gaussians  $f_0(J) = (1/2\pi D^2)^{1/2} \exp(-J^2/2D^2)$  centered at the centre of the island and of characteristic lengths  $D$  equal to half the island width  $D=w/2$  in Fig. 4(a) and one island width  $D=w$  in Fig. 4(b). (ii) Two

"step-like" distributions of the form  $f_0(J) = (1/\alpha D)^{1/2} \exp(-(J/\alpha D)^N)$  with  $N=16$ . Selecting  $\alpha = (N/N-1)^{1/N}$  places the sharp gradient at  $J=D$  and we plot the case  $D=w/2$  in Fig. 4(c) and  $D=w$  in Fig. 4(d).

Comparing Fig. 4(a) to Fig. 4(b) and Fig. 4(c) to Fig. 4(d) it is seen that the growth rates between similar types of distributions tend to decrease as the location of the maximum gradient  $(df_0/dJ)_{\max}$  approaches the separatrix. In both cases there is more than one order of magnitude reduction in the gain by shifting the maximum gradient position from  $D=w/2$  to  $D=w$ . Because  $f_0$  was chosen monotonic in all above plots and because it was limited to trapped particles,  $df_0/d\omega_b$  preserves sign and only lower modes are unstable. The spectral width of the unstable regimes is reduced with a parallel increase in the maximum gain as one goes from the Gaussian type to the step-like type of distributions. Also the distance of the sideband frequencies from the main signal decreases by shifting the gradient position  $D$  closer to the separatrix. Distributions with sharp gradients at the separatrix such as those in Figs. 4(b) and 4(d) are perhaps more relevant to the case of variable wiggler FEL, where the "bucket" of the trapped particles is decelerating in phase space leaving the untrapped particles behind, and only small diffusion occurs across the separatrix allowing sharp gradients.

The limit of a  $\delta$ -function distribution  $f_0 = \delta(J-J_0)$ , examined elsewhere<sup>13</sup>, is the most unstable case but of the least practical interest, because even the case of a monoenergetic beam distribution  $p_z = p_0$  is described in  $J$ -space by a smooth distribution  $f_0(J)$  of finite width  $\Delta J$  (see Fig. 1).

Our calculations done for the case of a fixed wavelength



wiggler can be easily extended to the case of a variable wiggler FEL provided that the same adiabatic assumptions hold. Only the functional relations Eqs. (7) between the action-angle variables  $(J, \theta)$  and the coordinates  $(P, \psi)$  need to change. The derivation of the growth rate, performed in  $J$ -space, is independent of the transformation  $J(P, \psi)$  and the result, Eq. (16), stands as is. It is the high gain of tapered wiggler FELs that seems to challenge the adiabatic approach to the problem. In this case the change of the signal amplitude  $a_r(t)$  in time together with the dependence of the pseudo-equilibrium  $f_0$  on both time and  $\theta$  should be included for a more realistic treatment.

#### Acknowledgements

This work was supported by the U. S. Army Strategic Defense Command.

## REFERENCES

1. N.M. Kroll, P.L. Morton and M.N. Rosenbluth, *IEEE J. Quantum Electron.* QE-17, 1436 (1981)
2. N.M. Kroll, P.L. Morton and M.N. Rosenbluth, *Free Electron Generators Coherent Radiation, Physics and Quantum Electronics*, Vol.7 (Reading, MA. Addison-Wesley) pg. 147 (1980).
3. W.B. Colson, *Phys. Quantum Electron.*, Vol.8 (Reading, MA. Addison-Wesley) pg.457 (1982).
4. W.B. Colson, *Proc. Seventh Int. Conf. on FELs*, (North Holland, E.T. Scharlemann, D. Prosnitz eds.) pg. 168(1985); also W.B. Colson, *Proc. Int. Conf. on Lasers*, (STS Press, Mc Lean VA) pg. 751 (1982).
5. T. Masud, T.C. Marshall, S.P. Schlesinger and F.G. Yee, *Phys. Rev. Lett.* 56, 1567 (1986).
6. T. Masud, T.C. Marshall, S.P. Schlesinger, F.G. Yee, W.M. Fawley, E.T. Scharleman, S.S. Yu, A.M. Sessler and E.J. Sternbach, to be published.
7. C.M. Tang and P. Sprangle in *Free Electron Generators of Coherent Radiation* (S.F. Jacobs, M.O. Scully, eds.) SPIE 453, pg.11 (1983).
8. D.C. Quimby, J.M. Slater and J.P. Wilcoxon, *IEEE J. Quantum Electron.* 21, 979 (1985).
9. M.N. Rosenbluth, H.V. Wong and B.N. Moore in *Free Electron Generators of Coherent Radiation* (S.F. Jacobs, M.O. Scully, eds.) SPIE 453, pg.25 (1983).
10. T.C. Marshall, private communication (1986).
11. R.C. Davidson, *Phys. Fluids* 29, 2689 (1986)
12. B. Lane and R.C. Davidson, *Phys. Rev. A* 27, 2008 (1983).
13. S. Riyopoulos and C. M. Tang, "Structure of the unstable sideband spectrum in FELs", submitted for publication.

## FIGURE CAPTIONS

**Figure 1.** Time averaged motion without the sidebands. (a) Plots in phase space of the unperturbed orbits  $H_0(P, \psi) = K$ . The intersections with the horizontal line  $P = \text{const.}$  mark the initial conditions for each orbit. (b) The normalized bounce frequency  $\omega_b$  and the first two harmonics as functions of the trapping parameter  $\lambda^2(J)$ . The intersections with the horizontal line  $\omega = (\omega_s - \omega_r)k_v/k_r$  determine the position  $J_n$  of the resonant orbits for a given  $\omega_s$ .

**Figure 2.** Gain for a Gaussian distribution  $f_0(J) = C \exp(-(J - J_0)^2 / 2D^2)$  centered halfway inside the trapped particle island  $J_0 = v/2$  and of width  $D$  equal to  $v$  where  $v = J_{\text{sep}}$ . The normalized gain  $g_s/\omega_r$  is plotted versus  $\delta\omega/\omega_r$  for (a) the fundamental contribution  $n=1$  in Eq. (16), (b) including the first harmonic  $n=2$ , (c) two harmonics and (d) three harmonics. The most unstable modes do not correspond to harmonics of the bounce frequency at the bottom  $\omega_b(0)$  indicated by the arrows.

**Figure 3.** Plot of  $df_0(J)/d\omega_b(J) = df_0/dJ (d\omega_b/dJ)^{-1}$  as a function of  $K(J) - K(0)$  for the distribution  $f_0$  of Figure 2. The slope goes to zero near the separatrix  $K(J_{\text{sep}})$  because of the infinite shear  $d\omega_b/dJ$ .

**Figure 4.** Normalized gain for monotonic distributions centered at the bottom of the well  $J=0$  including the first three harmonics  $n \leq 4$  in Eq. (16). (a) Gaussian distribution of width  $D$  equal to half the island width  $v$ ,  $D=v/2$  (b) Gaussian distribution with  $D=v$ . (c) Step-like distribution with  $D=v/2$  and (d) Step-like distribution with  $D=v$ .

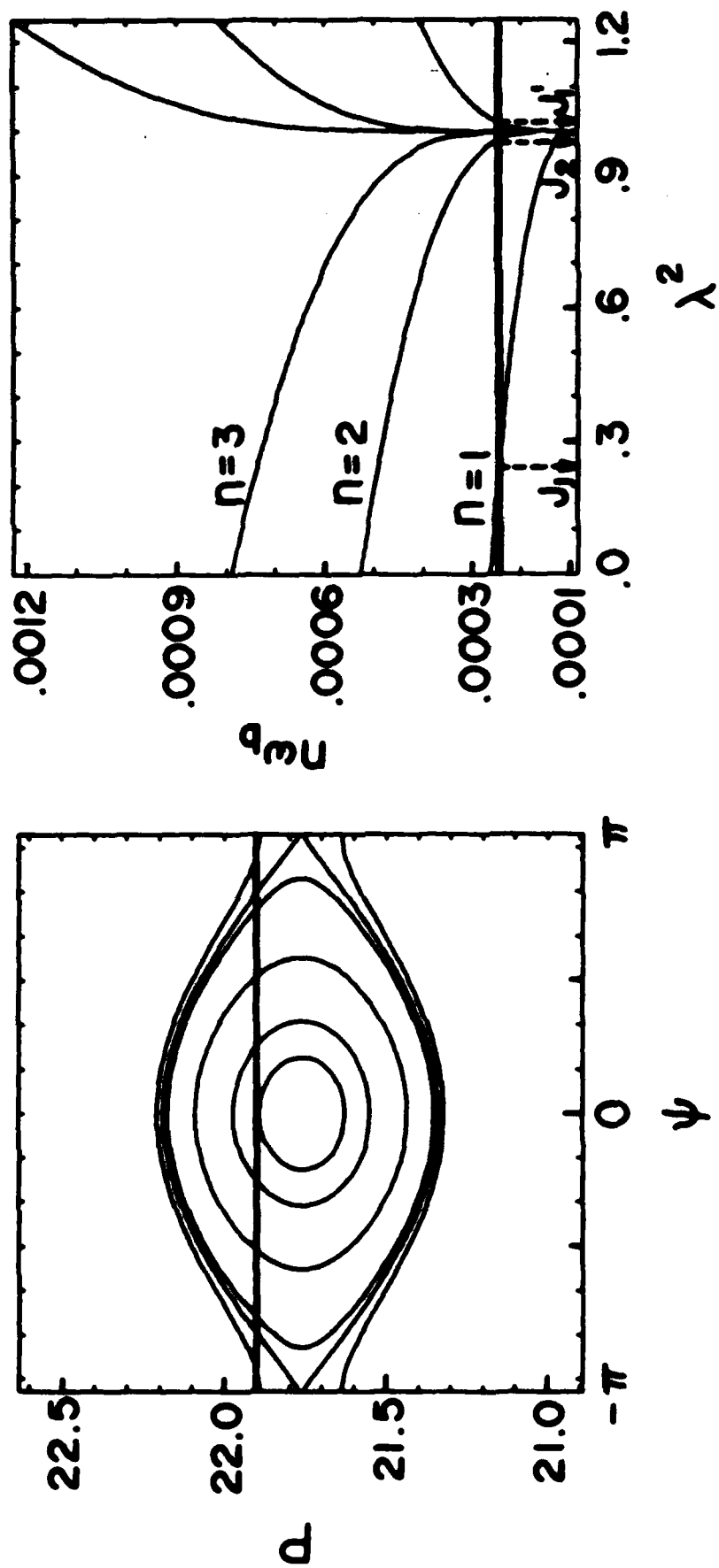


Fig. 1

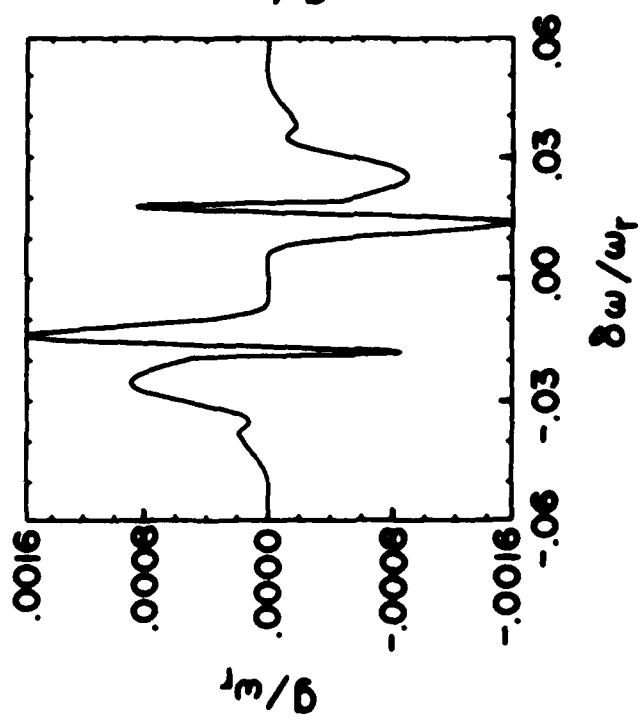
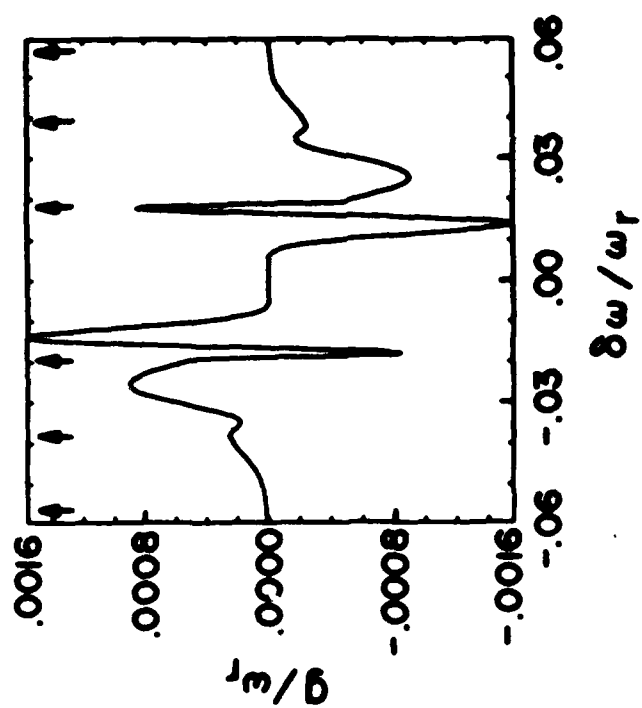
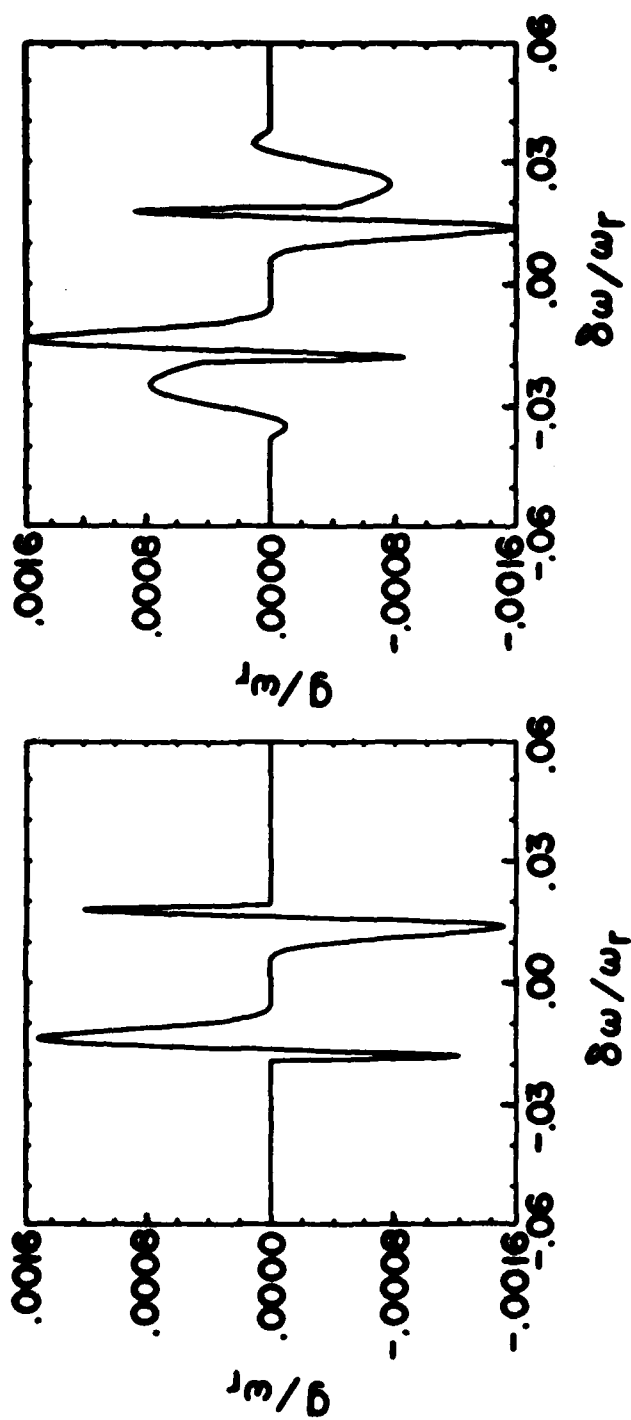


Fig. 2

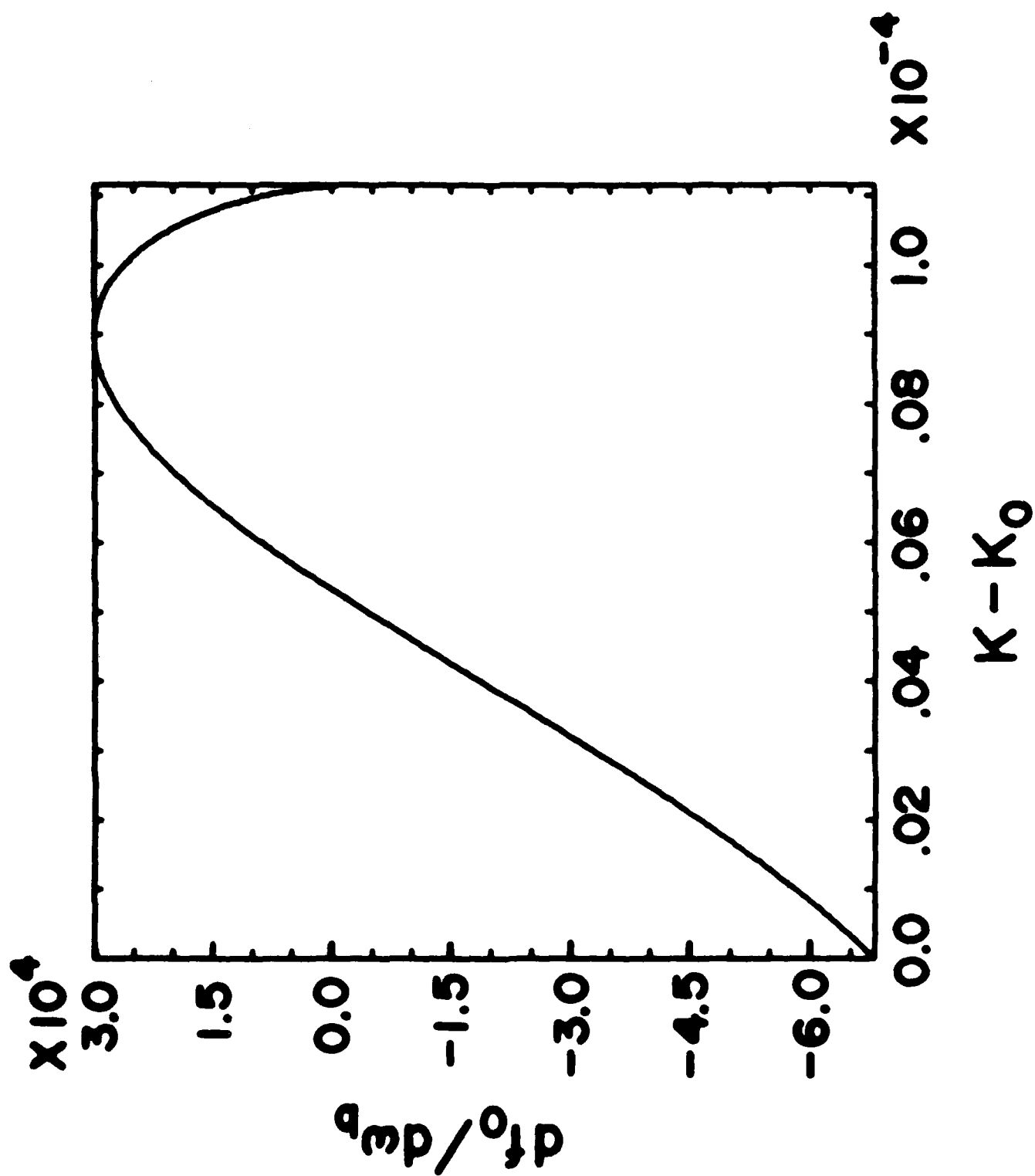


Fig. 3

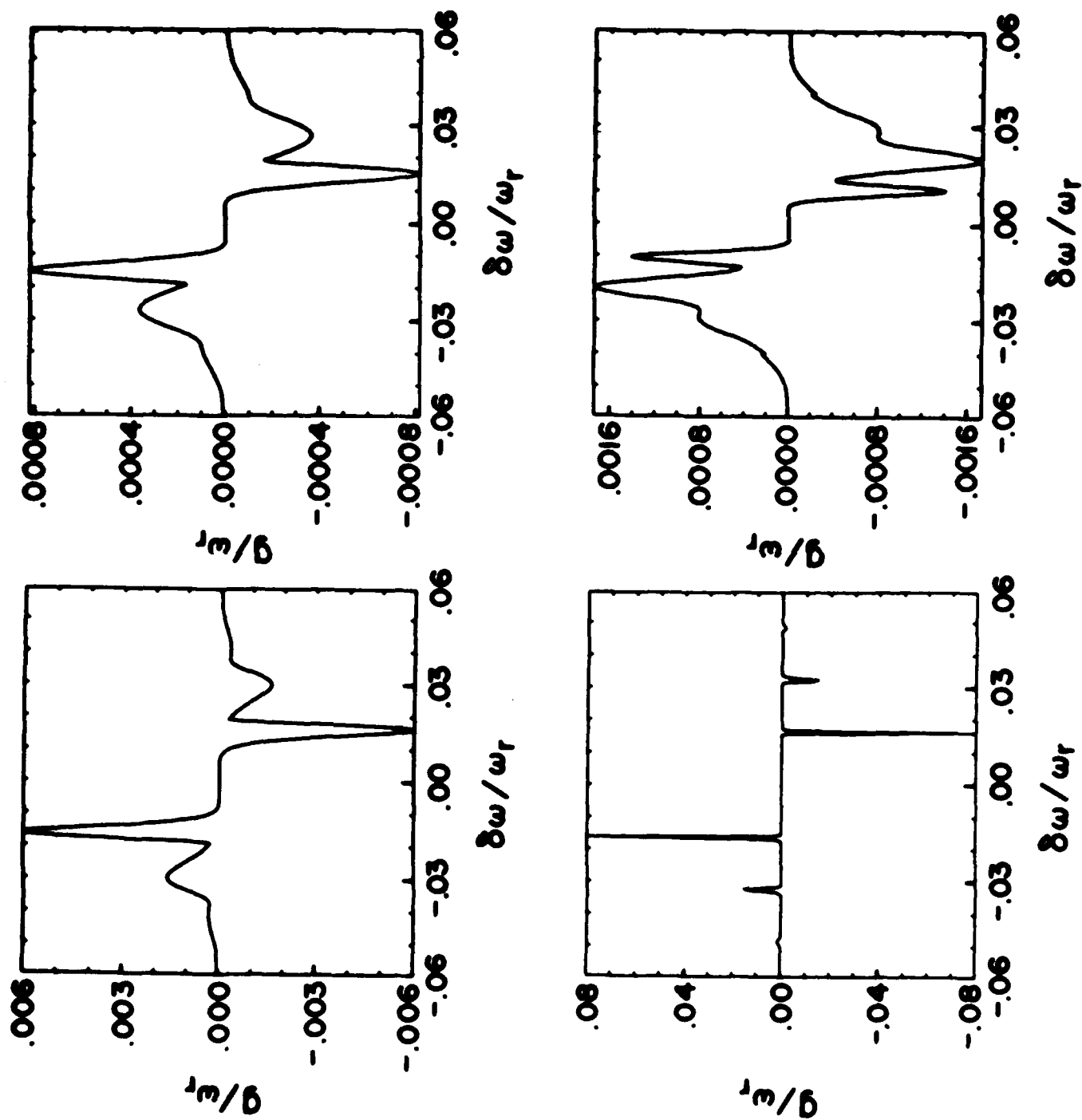


Fig. 4

END

7-87

DTIC